International Symposium
On Turbulence and Shear Flow
Phenomena (TSFP-9)
June 30 - July 3, 2015 *Melbourne, Australia*

ANALYTICAL AND NUMERICAL ANALYSES OF ENERGY TRANSFER AROUND ELLIPTICAL BURGERS VORTICES FOR LES

Hiromichi Kobayashi
Department of Physics
Keio University
4-1-1 Hiyoshi, Kohoku-ku, Yokohama, Kanagawa 223-8521, Japan
hkobayas@phys-h.keio.ac.jp

ABSTRACT

The energy transfer from large-scale to small-scale around elliptical Burgers vortices is analytically and numerically examined. The elliptical Burgers vortex is constructed by a background straining flow to the Burgers vortex, so that the Burgers vortex becomes non-axisymmetric. By taking a spatial filter to the elliptical Burgers vortices, we obtain the filtered velocity field. In large eddy simulation (LES), understanding the energy transfer from resolved-scale to subgrid-scale (SGS), the so-called forward scatter (FS) and backward scatter (BS), around the eddy is important. The SGS stress tensor is decomposed to Leonard, cross and Reynolds terms. Those contributions to the energy transfer are discussed. The FS region of the Leonard term appears along the major axis of the elliptical Burgers vortex. For cross and Reynolds terms, the FS regions emerge along the minor axis. The Reynolds term has much smaller intensity than the cross term. The SGS energy transfer distributions due to modified Leonard, cross and Reynolds terms, Bardina models and Smagorinsky model are discussed. This simple and analytical *a priori* test is useful to understand the feature of the decomposed and modelled terms for the SGS energy transfer.

INTRODUCTION

Vortex tubes, in other words, coherent eddies or energy containing eddies, emerge in turbulence. The coherent eddies in direct numerical simulation (DNS) are well approximated by the Burgers vortex (see, e.g., Tanahashi *et al*., 1994; Das *et al*., 2006; Wang *et al*., 2007). The high energy dissipation region in DNS has a double-peak structure around the eddy (Tanahashi *et al*., 1994; Kida & Ohkitani, 1992). The change of the double-peak structure with Reynolds number is numerically explained using a non-axisymmetric strained vortex (Kida & Ohkitani, 1992); here we call it the elliptical Burgers vortex. Moreover, the elliptical Burgers vortices are analytically solved under the large-Reynolds-number asymptotics, and the Reynolds number dependence of the high energy dissipation region is well reproduced (Moffatt *et al*., 1994).

In large eddy simulation (LES), the energy transfer between large-scale and small-scale is of great importance. The energy transfer from large-scale to small-scale, the so-called forward scatter, around the eddy occurs at the different location of the high energy dissipation as shown in DNS (Aoyama *et al*., 2005). The high forward scatter region has also a double-peak structure around the eddy in the log layer of wall turbulence experiments (Natrajan & Christensen, 2006). In order to consider the energy transfer, the analytical approach is useful to understand the feature of the energy transfer between the scales.

In this study, the energy transfer around the elliptical Burgers vortices is analytically and numerically examined. The energy transfer through the Leonard, cross, Reynolds terms decomposed from the subgrid-scale (SGS) stress tensor is also reproduced and those structures are discussed.

ANALYTICAL AND NUMERICAL METHODS

We use the analytical solution of the elliptical Burgers vortex (Moffatt *et al*., 1994) for the background straining flow $U = (\alpha x, \beta y, \gamma z)$ where $\alpha+\beta+\gamma = 0$, $\alpha < 0 < \gamma$, $\beta > \alpha$. The strain parameter is selected based on the DNS results (Wang *et al*., 2007); $\lambda = (\alpha-\beta)/(\alpha+\beta) = 9$, $\alpha = -(1+\lambda)/2 = -5$, $\beta = -(1-\lambda)/2 = 4$. The axis of the vortex aligns in z direction. The vorticity of the Burgers vortex for $\alpha = \beta$ is denoted as

$$\omega(r) = \frac{\gamma\Gamma}{4\pi\nu}\exp\left(-\frac{\gamma r^2}{4\nu}\right), \quad Re_\Gamma = \Gamma/\nu \tag{1}$$

where Γ is circulation, ν is viscosity, and Re_Γ is Reynolds number.

Velocities u_x and u_y in x and y directions and vorticity ω are defined with stream function ψ.

$$u_x = \partial\psi/\partial y, \quad u_y = -\partial\psi/\partial x \tag{2}$$

$$\omega = \frac{\partial u_y}{\partial x} - \frac{\partial u_x}{\partial y} = -\nabla^2\psi \tag{3}$$

$$\Gamma = \int\int \omega(x,y)dxdy \tag{4}$$

Steady vorticity equation is obtained as

$$(\alpha x+u_x)\frac{\partial\omega}{\partial x} + (\beta y+u_y)\frac{\partial\omega}{\partial y} = \gamma\omega + \nu\nabla^2\omega \tag{5}$$

When we normalize the above equation with

$$(x^*,y^*) = (x,y)/\delta, \quad (\alpha^*,\beta^*) = (\alpha,\beta)/\gamma,$$
$$\psi^* = \psi/\Gamma, \quad \delta = (\nu/\gamma)^{1/2} \tag{6}$$

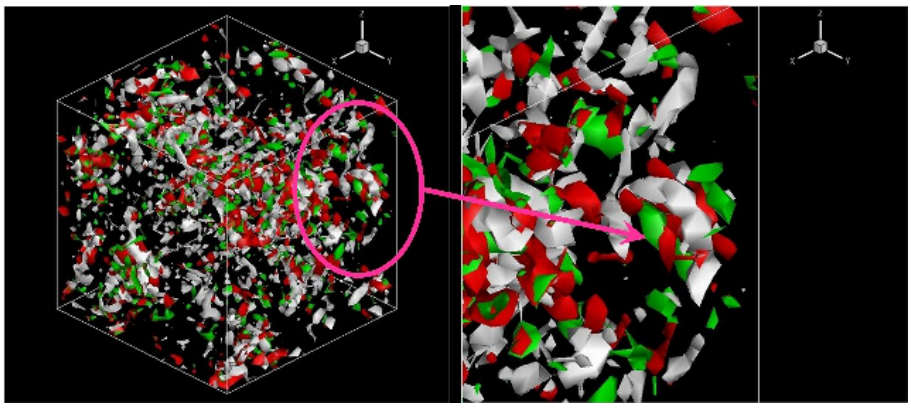

Figure 1. Eddies $Q = 100$ (white), negative Q region $Q = -100$ (green) and forward scatter region $-\tau_{ij}\overline{S}_{ij} = 80$ (red) at $Re_\lambda = 60$.

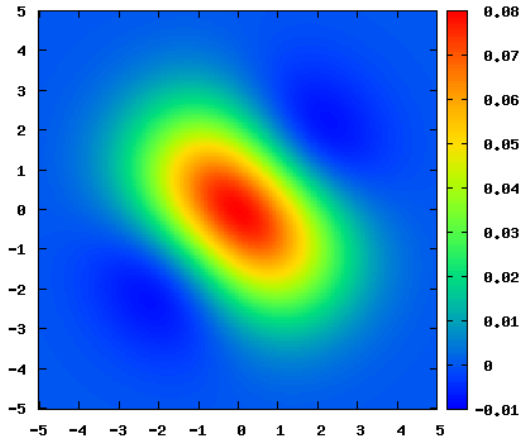

Figure 2. Analytical vorticity distribution of the elliptical Burgers vortex at $Re_\Gamma = 500$ with $\alpha : \gamma : \beta = -5 : 1 : 4$.

We obtain a normalized steady vorticity equation

$$\frac{\partial(\psi,\omega)}{\partial(x,y)} = \varepsilon\left[\left(\alpha x\frac{\partial}{\partial x}+\beta y\frac{\partial}{\partial y}\right)\omega-\omega-\nabla^2\omega\right] \quad (7)$$

$$\psi = \psi_0(r)+\varepsilon_1 f(r)\sin 2\theta+\varepsilon^2\psi_2(r,\theta) \quad (8)$$

$$f''+r^{-1}f'-4r^{-2}f = -(f-r^2/4)r^2/[4(e^{r^2/4}-1)] \quad (9)$$

$$\omega_0(r) = \frac{1}{4\pi}e^{-r^2/4} \quad (10)$$

$$\varepsilon = 1/Re_\Gamma = \nu/\Gamma \ll 1, \quad \varepsilon_1 = \lambda\varepsilon \quad (11)$$

In the present study, we use $\varepsilon = 1/Re_\Gamma = 1/500$.

In order to obtain the filtered velocity field, we use a differential filtering with $\overline{\Delta} = 5/4 r_{max}$,

$$\overline{u}_i = u_i + \frac{\overline{\Delta}^2}{24}\Delta u_i + O(\overline{\Delta}^4), \quad u_i = \overline{u}_i + u_i'' \quad (12)$$

where $r_{max} = 2.2418$ is the radius at maximum azimuthal velocity for ω_0.

As a result, the energy transfer for the forward scatter

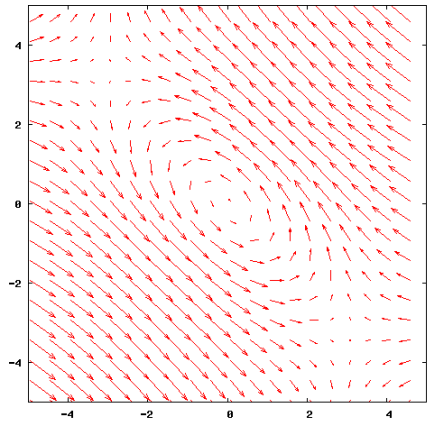

Figure 3. Velocity vectors around the elliptical burgers vortex.

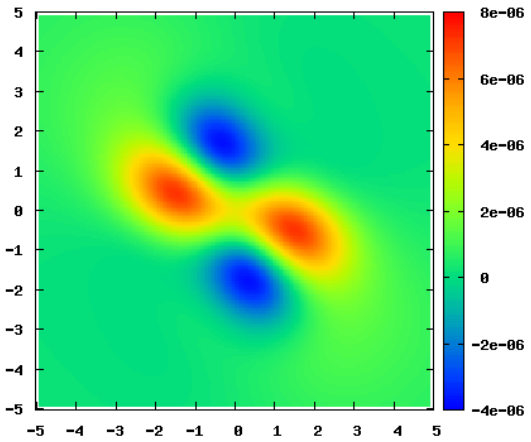

Figure 4. Analytical distribution of the SGS energy transfer $(-\tau_{ij}\overline{S}_{ij})$ around the elliptical Burgers vortex.

is defined as

$$-\tau_{ij}\overline{S}_{ij} > 0, \quad \tau_{ij} = \overline{u_i u_j} - \overline{u}_i\overline{u}_j, \quad \overline{S}_{ij} = \frac{1}{2}\left(\frac{\partial\overline{u}_j}{\partial x_i}+\frac{\partial\overline{u}_i}{\partial x_j}\right) \quad (13)$$

where τ_{ij} is the SGS stress tensor, $\overline{S}_{ij}$ is the velocity strain

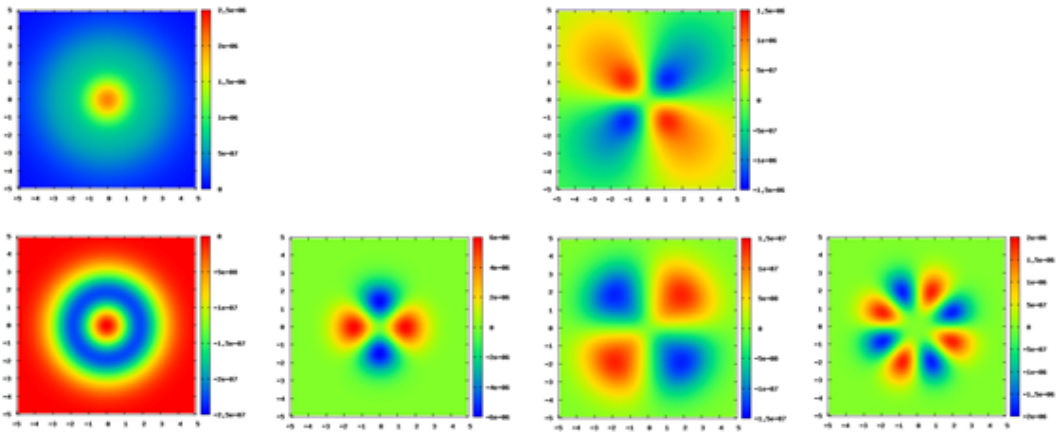

Figure 5. Decomposed distributions the SGS energy transfer ($-\tau_{ij}\overline{S}_{ij}$) denoted in Eq. (25); the terms including $D_0(r)$ (upper left), $D_2(r)$ (upper right), $E_0(r)$, $E_1(r)$, $E_2(r)$ and $E_3(r)$ (lower).

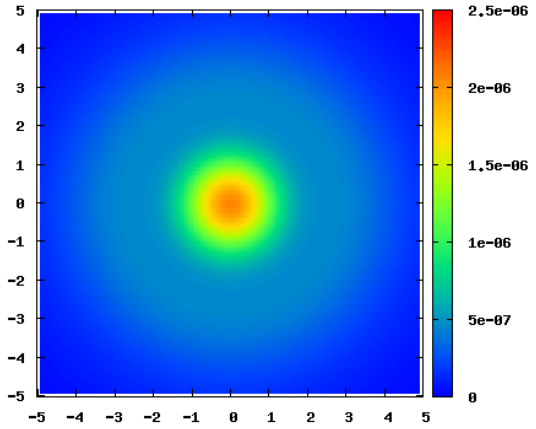

Figure 6. Energy transfer distribution of net FS for $-\tau_{ij}\overline{S}_{ij}$.

tensor, and the overline (-) shows filtered variables for a resolved scale. A filtering operation with the finite difference method is adopted. The SGS stress tensor is decomposed into the Leonard term L_{ij}, the cross term C_{ij}, and Reynolds term R_{ij} with $u_i = \overline{u}_i + u_i''$ as follows.

$$\tau_{ij} = L_{ij} + C_{ij} + R_{ij} \tag{14}$$
$$L_{ij} = \overline{\overline{u}_i \overline{u}_j} - \overline{u}_i \overline{u}_j \tag{15}$$
$$C_{ij} = \overline{\overline{u}_i u_j''} + \overline{u_i'' \overline{u}_j} \tag{16}$$
$$R_{ij} = \overline{u_i'' u_j''} \tag{17}$$

Germano (1986) modified the above terms to satisfy the Galilean invariance as follows.

$$\tau_{ij} = L_{ij}^m + C_{ij}^m + R_{ij}^m \tag{18}$$
$$L_{ij}^m = \overline{\overline{u}_i \overline{u}_j} - \overline{\overline{u}}_i \overline{\overline{u}}_j \tag{19}$$
$$C_{ij}^m = \overline{\overline{u}_i u_j''} - \overline{\overline{u}}_i \overline{u_j''} + \overline{u_i'' \overline{u}_j} - \overline{u_i''}\,\overline{\overline{u}}_j \tag{20}$$
$$R_{ij}^m = \overline{u_i'' u_j''} - \overline{u_i''}\,\overline{u_j''} \tag{21}$$

Bardina (1980) proposed a model using GS (resolved) velocity for the cross and Reynolds terms.

$$C_{ij}^B = \overline{\overline{u}}_i \left(\overline{u}_j - \overline{\overline{u}}_j\right) + \left(\overline{u}_i - \overline{\overline{u}}_i\right) \overline{\overline{u}}_j (\approx C_{ij}) \tag{22}$$
$$R_{ij}^B = \left(\overline{u}_i - \overline{\overline{u}}_i\right) \left(\overline{u}_j - \overline{\overline{u}}_j\right) (\approx R_{ij}) \tag{23}$$
$$\tau_{ij} \approx L_{ij} + C_{ij}^B + R_{ij}^B = L_{ij}^m \tag{24}$$

DNS of 128^3 is carried out at $Re_\lambda = 60$ based on Taylor micro scale for homogeneous isotropic turbulence with the fourth-order central finite difference method. The domain size is $2\pi \times 2\pi \times 2\pi$ and the periodic boundary condition is used. The MAC scheme is adopted for the coupling of velocity and pressure and the Poisson equation for pressure is solved by using FFT method. The third order Adams-Bashforth method is used for time marching scheme. The resolved scale variable for LES of 32^3 is produced with a Gaussian filter of filter width $2\pi/27$ (Kobayashi, 2005).

RESULTS

Figure 1 shows the resolved-scale eddies extracted with the second invariance Q of velocity gradient tensor (white, positive Q; green, negative Q) and the forward scatter (FS) region (red). The positive Q shows the eddy structure, while the negative Q region has a double-peak structure. The forward scatter region well correlates with the negative Q region and has also a double-peak structure. This fact is consistent with the result in the wall turbulence experiment (Natrajan & Christensen, 2006).

The analytical vorticity distribution of the elliptical Burgers vortex at $Re_\Gamma = 500$ with $\alpha : \gamma : \beta = -5 : 1 : 4$ is shown in Fig. 2. Figure 3 shows the velocity vectors around the elliptical Burgers vortex. These distributions are consistent with the DNS results (Wang *et al.*, 2007).

Figure 4 shows an analytical distribution of the SGS energy transfer ($-\tau_{ij}\overline{S}_{ij}$) around the elliptical Burgers vortex. Red colour shows the FS region and Blue colour shows the backward scatter (BS) region. Those regions have double peak structures. The SGS energy transfer distribution is similar to that obtained in a log layer of wall turbulence experiments (Natrajan & Christensen, 2006). The FS appears the velocity field from major axis to minor one, whereas the BS emerges that from minor axis to major one.

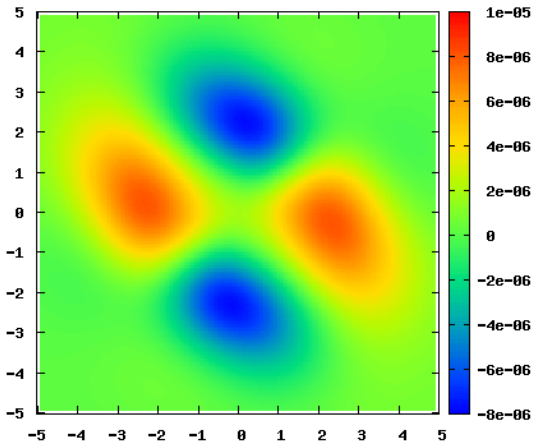

Figure 7. SGS energy transfer through the Leonard term ($-L_{ij}\overline{S}_{ij}$).

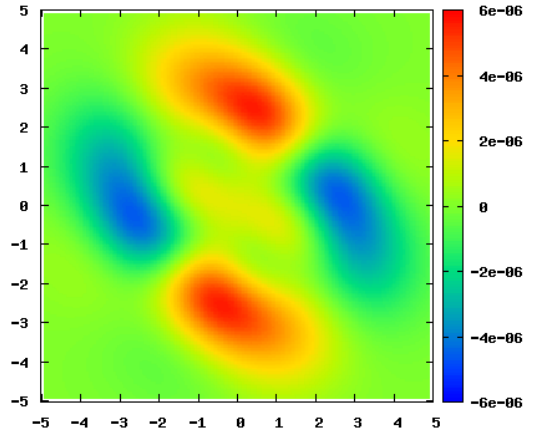

Figure 8. SGS energy transfer through the cross term ($-C_{ij}\overline{S}_{ij}$).

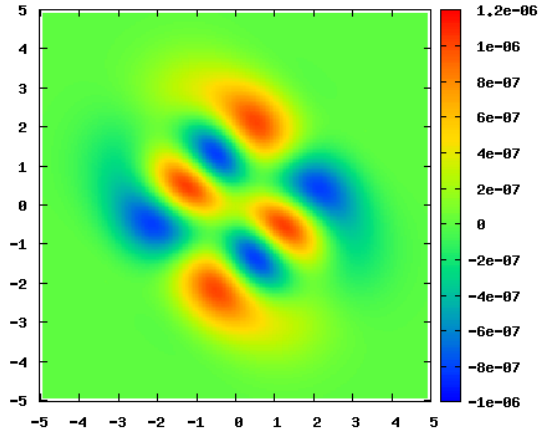

Figure 9. SGS energy transfer through the Reynolds term ($-R_{ij}\overline{S}_{ij}$).

Figure 5 shows the decomposed distributions into the terms denoted in the following equation.

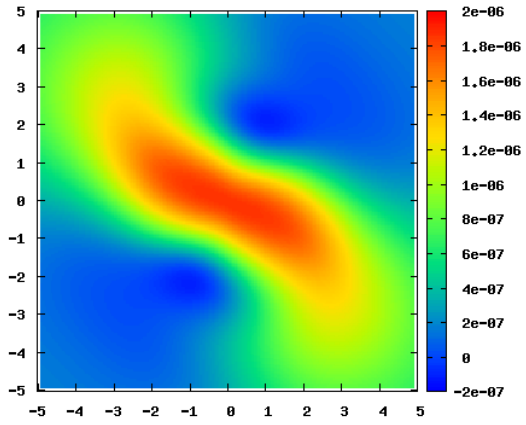

Figure 10. SGS energy transfer through the modified Leonard term ($-L^m_{ij}\overline{S}_{ij}$).

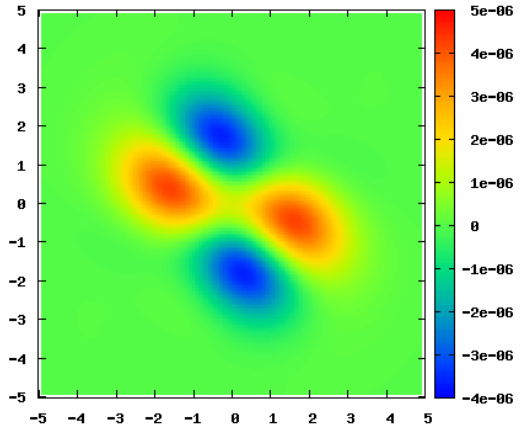

Figure 11. SGS energy transfer through the modified cross term ($-C^m_{ij}\overline{S}_{ij}$).

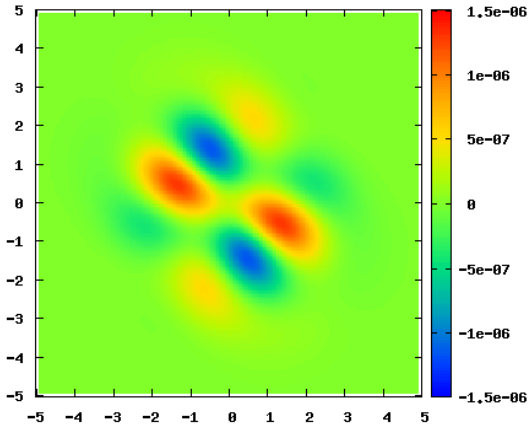

Figure 12. SGS energy transfer through the modified Reynolds term ($-R^m_{ij}\overline{S}_{ij}$).

$$-\tau_{ij}\overline{S}_{ij} = \frac{\overline{\Delta}^2\varepsilon}{12}\left[D_0(r) + (\varepsilon_1 \sin 2\theta)\, D_2(r)\right] + \frac{\overline{\Delta}^4\varepsilon}{288}\left[E_0(r) + (\lambda \cos 2\theta)\, E_1(r) + (\varepsilon_1 \sin 2\theta)\, E_2(r) + (\lambda\varepsilon_1 \sin 4\theta)\, E_3(r)\right] \quad (25)$$

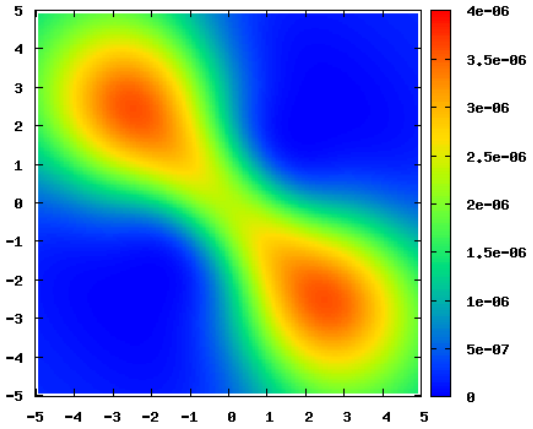

Figure 13. Energy transfer distribution with Smagorinsky model ($C_S = 0.1$).

Thus, if we integrate Eq. (25) in the plane, the terms with $D_2(r), E_1(r), E_2(r)$ and $E_3(r)$ are canceled out. Therefore, we obtain the following net FS with the terms of $D_0(r)$ and $E_0(r)$ and the distribution as shown in Fig. 6.

$$\int_0^{\infty}\int_0^{2\pi} -\tau_{ij}\overline{S}_{ij} r dr d\theta = \frac{\overline{\Delta}^2\varepsilon}{96\pi}\left[1 - \frac{5(\log 4 - 1)\overline{\Delta}^2}{768}\right] \tag{26}$$

Figures 7, 8 and 9 display the SGS energy transfer distributions of Leonard, cross and Reynolds terms from the analytical solution. The forward scatter region of the Leonard term appears along the major axis of the elliptical Burgers vortex. For cross and Reynolds terms, the forward scatter regions emerge along the minor axis. The Reynolds term has much smaller intensity than the cross term. Horiuti (1989) showed inverse correlations between L_{12} and C_{12} in a channel flow. That result is consistent with our result as shown in Figs. 7 and 8.

The SGS energy transfer $-\tau_{ij}\overline{S}_{ij}$ is decomposed into the modified terms proposed by Germano (1986). Figures 10, 11 and 12 show the SGS energy transfer distributions of modified Leonard, modified cross and modified Reynolds terms. The energy transfer distribution due to the cross term ($-C_{ij}\overline{S}_{ij}$) inversely correlates with the modified cross term ($-C^m_{ij}\overline{S}_{ij}$). Horiuti (1997) showed good correlations between L^m_{ij} and C^m_{ij} in a channel flow and a mixing layer. That result is consistent with our result as shown in Figs. 10 and 11. Salvetti & Banerjee (1995) showed good correlations among $\tau_{ij}\overline{S}_{ij}$, $L^m_{ij}\overline{S}_{ij}$ and $C^m_{ij}\overline{S}_{ij}$. Those results are supported with our results in Figs. 4, 10 and 11.

If we use Smagorinsky model

$$\tau_{ij} = -2C_S|\overline{S}|\overline{S}_{ij}, \quad (|\overline{S}| = \sqrt{2\overline{S}_{ij}\overline{S}_{ij}}) \tag{27}$$

wih the model constant $C_S = 0.1$, we get the energy transfer distribution as shown in Fig. 13.

When we use Bardina models for the cross and Reynolds terms, we obtain the energy transfer distributions as shown in Figs. 14 and 15. The energy transfer distribution of $-C^B_{ij}\overline{S}_{ij}$ well correlates with that of $-R^B_{ij}\overline{S}_{ij}$. The term C^B_{ij} is well modeled for the cross term C_{ij} in comparison with Figs. 8 and 14. Horiuti (1989) showed good correlations between C_{12} and C^B_{12} in a channel flow. That result is consistent with our result as shown in Figs. 8 and 14.

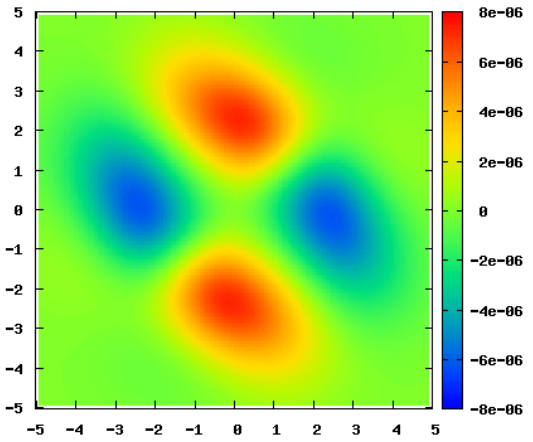

Figure 14. Energy transfer distribution with Bardina model (C^B_{ij}) for the cross term.

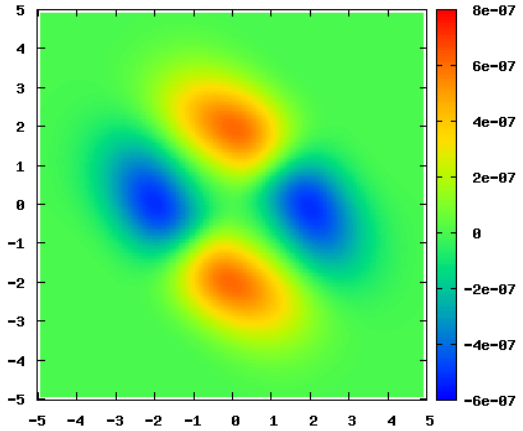

Figure 15. Energy transfer distribution with Bardina model (R^B_{ij}) for the Reynolds term.

SUMMARY

The SGS energy transfer around an elliptical Burgers vortex was examined analytically. The following results were obtained.

Forward scatter (FS) and backscatter (BS) have double peak structures. The FS appears the velocity field from major axis to minor one, whereas the BS emerges that from minor axis to major one. Net FS takes place at the centre of vortex, because those double peak structures are cancelled by integration of the SGS energy transfer in the azimuthal direction. The amount of the net FS is independent of the strain parameter λ, and has a peak with a filter width. From a decomposition to L_{ij}, C_{ij}, R_{ij}, the distribution of $L_{ij}\overline{S}_{ij}$ has negative correlation with that of $C_{ij}\overline{S}_{ij}$, and $R_{ij}\overline{S}_{ij}$ contributes a little to $\tau_{ij}\overline{S}_{ij}$. $C^m_{ij}\overline{S}_{ij}$ correlates inversely with $C_{ij}\overline{S}_{ij}$, and has good correlation with $\tau_{ij}\overline{S}_{ij}$.

H.K.'s work is supported by JSPS KAKENHI Grant Number 26420122, Grant-in-Aid Scientific research (C) in Japan Society for the Promotion of Science.

REFERENCES

Aoyama, T., Ishihara, T., Kaneda, Y., Yokokawa, M., Itakura, K. & Uno, A. 2005 Statistics of Energy Transfer in High-Resolution Direct Numerical Simulation of Turbulence in a Periodic Box. *Journal of the Physical Society of Japan* **74**, 12, 3202–3212.

Bardina, J. 1980 Improved turbulence models based on large eddy simulation of homogeneous, incompressible, turbulent flows. *Ph.D. dissertation* Stanford University.

Das, S. K., Tanahashi, M., Shoji, K. & Miyauchi, T. 2006 Statistical properties of coherent fine eddies in wall-bounded turbulent flows by direct numerical simulation. *Theor. Comp. Fluid Dyn* **20**, 2, 55–71.

Germano, M. 1986 A proposal for a redefinition of the turbulent stresses in the filtered Navier-Stokes equations. *Phys. Fluids* **29**, 2323–2324.

Horiuti K. 1989 The role of the Bardina model in large eddy simulation of turbulent channel flow. *Phys. Fluids A* **1**, 426–428.

Horiuti K. 1997 A new dynamic two-parameter mixed model for large-eddy simulation. *Phys. Fluids* **9**, 3443–3464.

Kida, S. & Ohkitani, K. 1992 Spatiotemporal intermittency and instability of a forced turbulence. *Phys. Fluids A* **4**, 1018–1027.

Kobayashi H. 2005 The subgrid-scale models based on coherent structures for rotating homogeneous turbulence and turbulent channel flow. *Phys. Fluids* **17**, 045104.

Moffatt, H. K., Kida, S. & Ohkitani, K. 1994 Stretched vortices – the sinews of turbulence; large-Reynolds-number asymptotics. *J. Fluid Mech.* **259**, 241–264.

Natrajan, V. K. & Christensen, K. T. 2006 The role of coherent structures in subgrid-scale energy transfer within the log layer of wall turbulence. *Phys. Fluids* **18**, 065104.

Salvetti, M. V. & Banerjee, S. 1995 *A priori* tests of a new dynamic subgrid-scale model for finite-difference large-eddy simulations. *Phys. Fluids* **7**, 2831–2847.

Tanahashi, M., Miyauchi, T. & Yoshida, T 1994 Characteristics of small scale vortices related to turbulent energy dissipation. In *Proceedings of the Ninth International Symposium on Transport Phenomena in Thermal-Fluids Engineering* **2**, 1256–1261.

Wang, Y., Tanahashi, M. & Miyauchi, T. 2007 Coherent fine scale eddies in turbulence transition of spatially-developing mixing layer. *Int. J. Heat and Fluid Flow* **28**, 6, 1280–1290.